DIAGNOSIS AND CHARACTERIZATION OF EFFECTS OF BROKEN BARS IN THREE PHASE SQUIRREL CAGE INDUCTION MOTOR USING FINITE ELEMENT METHOD

Nagarajan S. and RamaReddy S.
Department of Electrical and Electronics Engineering, Jerusalem College of Engineering, Anna University, Chennai, Tamil Nadu, India
E-Mail: nagu_shola@yahoo.com

ABSTRACT

Three Phase Induction Motors are widely used for industrial and domestic applications. There are various faults that occur in induction motors like stator inter-turn fault, bearing's faults and eccentricity fault. Out of these faults, the rotor broken bar fault is very specific in squirrel cage induction machines. This paper deals with the detection of broken bars in three phase squirrel cage induction motor using finite element model of the induction machine. Finite element method is more precise than the winding function approach method, as it is based on the actual geometry of the machine. This paper uses a CAD package called "Magnet" for the Static 2D and Transient 2D analysis. The various machine parameters like flux density, flux function, magnetic energy, etc are calculated using this CAD package and their values are compared under healthy and faulty conditions.

Keywords: rotor broken bars, finite element method, induction motor, magnet, flux density, flux function, magnetic energy.

INTRODUCTION

Three phase induction motors have wide applications in various industries. It is recognized that a variety of faults can occur in these motors during normal operation such as rotor fault (broken bars or end ring), stator inter-turn fault, eccentricity fault and bearing fault. Hence early detection and diagnosis of such faults are very essential for the protection of induction motors against failures and permanent damages. A sudden motor failure may reduce productivity and may be catastrophic in an industrial system if undetected. In recent years, the problem of failures in large machines has become more significant. The desire to improve the reliability of the industrial drive systems has led to researches and developments in various countries to evaluate the cause and consequences of various fault conditions.

The interior faults of induction motor accounts for more than 70% in proportion of induction motor failures. Interior faults include stator and rotor faults of induction motors. Rotor faults are related to broken bars. Rotor failures are caused by a combination of various stresses that act on the rotor and these stresses can be identified as electromagnetic, thermal, dynamic, environmental and mechanical. Therefore these leads to low-frequency torque harmonics, which increases noise and vibration.

The transient analysis was done using coupled electric circuit with 2D finite element electromagnetic field analysis. The designed geometric dimension is modeled in the finite element domain and transient performances are predicted at the starting of motor with no load [1]. An MCSA technique is adopted for the diagnosis of rotor breakages in squirrel cage induction motor and finite method to calculate the parameters and modeled using state space modeling approach. It computes the characteristic frequency components which are indicative of rotor bar and connector breakages and developed torque profiles [2].

A local approach was proposed to tackle the problems of breaking bars and end rings. It was implemented by CAD software, Flux 2D and allows better accuracy and simpler mode of detection [3]. The analysis of a three phase induction motor fed by a symmetric three phase AC voltage source is done using two different approaches. The first method is based on the electrical circuit of the motor and the second method is based on the field solution. Both the approaches implemented in Ansoft Maxwell and Cedrat Flux 2D [4]. Broken bars are detected using experimental set ups and computation were done using non-linear complex steady state technique [5].

The effect of adjacent and non adjacent bar breakages was done in squirrel cage induction machines. It describes how the non adjacent bar breakages result in the masking of fault indices and problems related to it [6]. A corrosion rotor bar model was derived from electromagnetic field theory and simulated using Matlab Simulink [7]. Detection of dynamic, static eccentricities and bar, end-ring connector breakages is done using Time-Stepping Coupled Finite-Element State Space method and generates the fault case performance data which contain the phase current waveforms and tine domain torque profiles [8].

The optimization of Fractional Fourier Transform was proposed to generate a spectrum where the frequence varying fault harmonics appears as a single spectral line and therefore facilitate the diagnostic process [9]. A new technique based on rotor magnetic field space vector orientation was proposed to diagnose the broken bar faults at steady state [10].

The behavior of three phase induction motor with internal fault condition under sinusoidal supply voltage was examined by discrete wavelet transform and extracts the different harmonic components of stator currents [11]. Equivalent circuit approach usually gives adequate predictions of torque and current but gives no information on flux distribution. This deficiency is overcome by numerical approach which uses 2D, nonlinear, time stepping finite element method for excitation from a constant voltage source [12].

The effect of pole pair and rotor slot numbers was presented under different harmonics in healthy and eccentric conditions. The simulation technique was not as accurate as Finite Element Method [13]. A dynamic model for IM under inter turn insulation failure fault was derived using reference frame theory. Finite element analysis is used for parameter determination of the machine in healthy and faulty condition [14]. An MCSA technique to diagnose the faults in the three phase induction motor drives was focused [15]. The use of Partial Relative Indexes (PRI) is proposed as a new fault indicator to ameliorate the reliability of fault detection task and uses MCSA method [16].

The above literature uses vibration monitoring techniques, MCSA, and Thermal Monitoring for the detection of faults. In this paper Finite element analysis is adopted to perform Static and Transient 2D analysis to detect the faults of three phase squirrel cage induction motor. The analysis is carried out with a CAD package called Magnet.

FINITE ELEMENT METHOD

Finite element analysis (FEA) is a computer based numerical technique for calculating the parameters of electromagnetic devices. It can be used to calculate the flux density, flux linkages, inductance, torque; induced emf etc., in the finite element method, the large electromagnetic device is broken down into many small elements. The behavior of an individual element can be described with a relatively simple set of equations. The equations describing the behavior of the individual elements are joined into an extremely large set of equations that describe the whole device. The computer can solve this large set of simultaneous equations. From the solution, the computer extracts the behavior of the individual elements. Finite element methods (FEM) of analysis have emerged in the past decades as the useful numerical methods for magnetic field analysis of electrical machines.

To determine the magnetic field distribution inside the motor, the following assumptions are made:

- The magnetic field outside the motor periphery is negligible.
- Hysteresis effects are neglected.
- The magnetic field distribution is constant along the axial direction of the motor.
- The displacement currents are neglected.

The energy stored in a current carrying coil is defined in (1).

$$W_m = \tfrac{1}{2} L I^2 \quad (1)$$

Table-1. Induction machine data.

Rated power	22KW
Rated voltage	415V
Rated line current	70.87A
Rated frequency	50Hz
Rated speed	1458 rpm
Number of poles	4
Number of stator slots	36
Number of rotor slots	28
Slip	0.028
Efficiency	0.85
Power factor	0.88

The induction machine data is given in Table-1. Each component of the field quantities is assumed to vary sinusoidal with time. The approach is based on field solution. The stator winding is a double cage winding and star connection is adopted. From the design data the average flux density is taken as 0.45 Wb/m^2. For good overall design, the ratio of length to pole pitch ratio is 1. The slots per pole per phase are assumed to be 3 and the air gap length is fixed to be 0.7mm.

Induction motor model

The model of an induction motor is shown in Figure-1. There are four steps involved in finite element analysis. They are Discretisation, Shaping Function, Stiffness matrix and Solution Technique. The steps involved in the CAD package are Pre processing where the discretisation of model is done, Solver and Post processing.

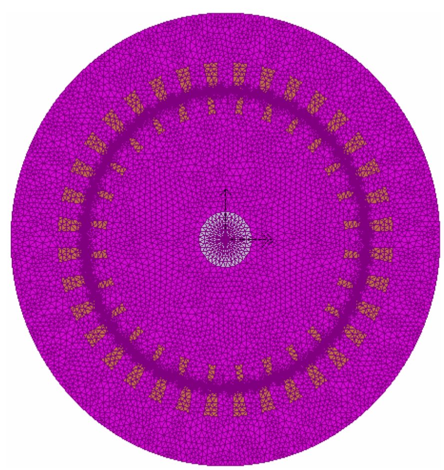

Figure-1. Discretisation of induction motor model.

First the original field problem domains are discretized or divided into number of sub domains or elements. The shaping function is defined at each node. To achieve minimization, it is convenient to separate the

 ISSN 1819-6608
ARPN Journal of Engineering and Applied Sciences

www.arpnjournals.com

global energy into its element components and to minimize one triangle at a time. Then appropriate solution technique is used to solve the equations and obtain the necessary parameters like energy, flux function, current, torque etc.

STATIC ANALYSIS

In this section, the simulation results for the Static Analysis of Three Phase Induction Motor for healthy motor, faulty motor with 2, 4, 6 and 8 broken bars under no load, half load and full load are presented.

Distribution of magnetic field and flux

Under the healthy conditions, the distribution of magnetic field is symmetrical, while the symmetry of magnetic field distribution is unsymmetrical in the case of broken bars and a higher degree of magnetic saturation can be observed around the broken bars.

Field and flux distribution plots for healthy and faulty motor under no load is shown in the Figure-2 and under full load is shown in Figure-3. It can be observed that plots appear to drastically change its symmetry when the number of broken bars in the rotor increases.

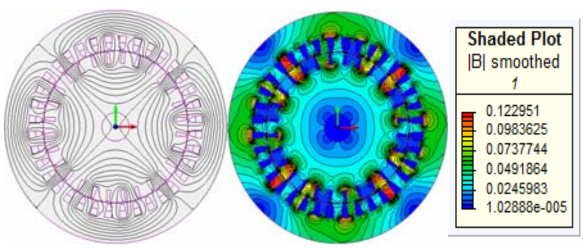

(a)

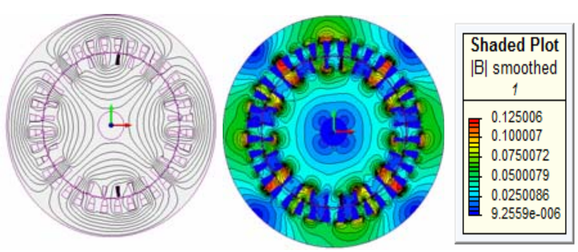

(b)

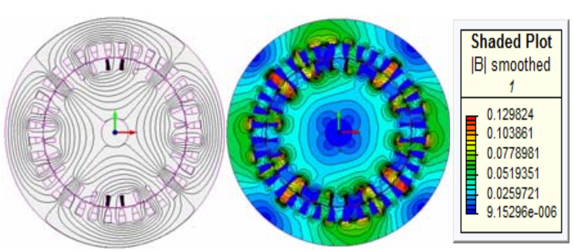

(c)

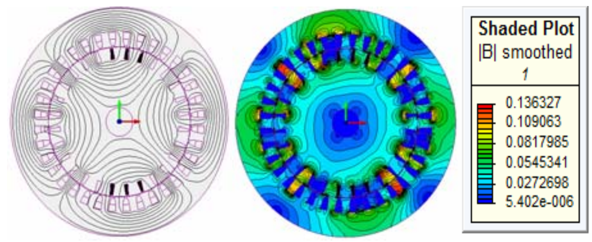

(d)

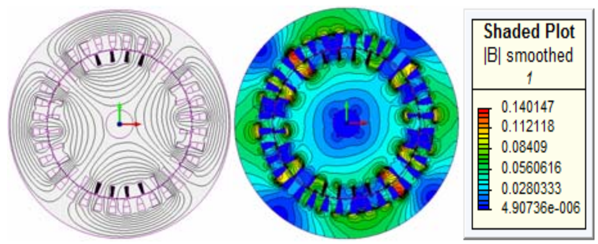

(e)

Figure-2. Magnetic field and flux distribution under no load (a) Healthy (b) 2 broken bar (c) 4 broken bar (d) 6 broken bar (e) 8 broken bar.

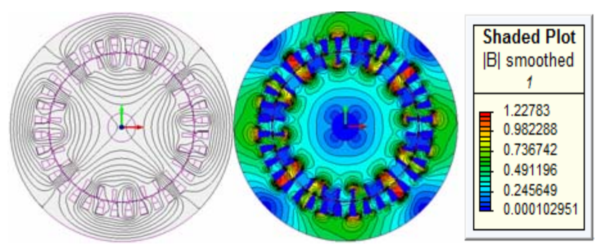

(a)

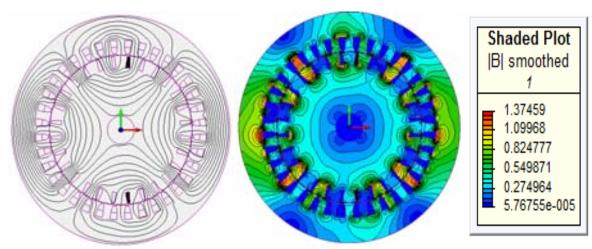

(b)

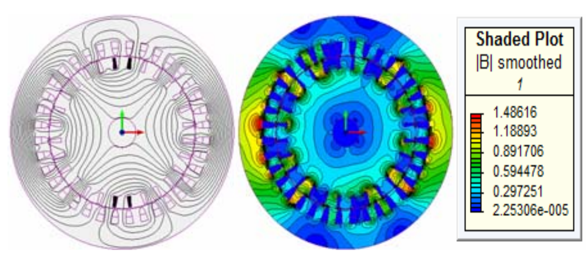

(c)

VOL. 7, NO. 9, SEPTEMBER 2012 ISSN 1819-6608
ARPN Journal of Engineering and Applied Sciences

www.arpnjournals.com

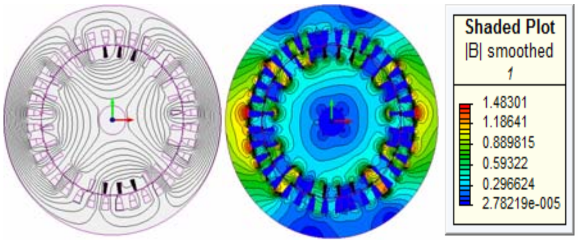

(d)

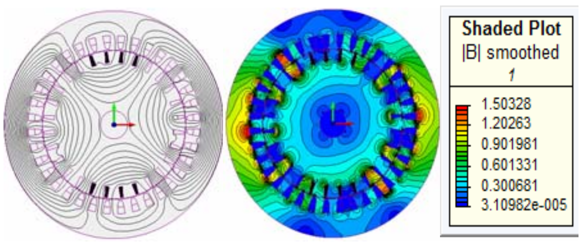

(e)

Figure-3. Magnetic field and flux distribution under full load (a) Healthy (b) 2 broken bar (c) 4 broken bar (d) 6 broken bar (e) 8 broken bar.

The stored magnetic energy under various loads is tabulated in Table-2. It can be observed that the stored magnetic energy reduced when the number of broken bars increases.

Table-2. Stored magnetic energy.

Condition		**Stored magnetic energy** (Joules)	**Percentage Change** (%)
No load	Healthy	0.0005013	-
	2 broken bar	0.0004984	0.58
	4 broken bar	0.0004939	1.48
	6 broken bar	0.0004871	2.83
	8 broken bar	0.0004783	4.58
Half load	Healthy	0.0273506	-
	2 broken bar	0.0270617	1.05
	4 broken bar	0.0266133	2.69
	6 broken bar	0.0259341	5.17
	8 broken bar	0.0250502	8.41
Full load	Healthy	0.0501441	-
	2 broken bar	0.0500637	0.16
	4 broken bar	0.0497823	0.72
	6 broken bar	0.0490010	2.28
	8 broken bar	0.0484359	3.40

Field and flux profile

The waveforms for field distribution and flux density for healthy and faulty motor under no load is shown in Figure-4 and under full load is shown in Figure-5. The flux density and flux function values under various loads are tabulated in Table-3 and Table-4.

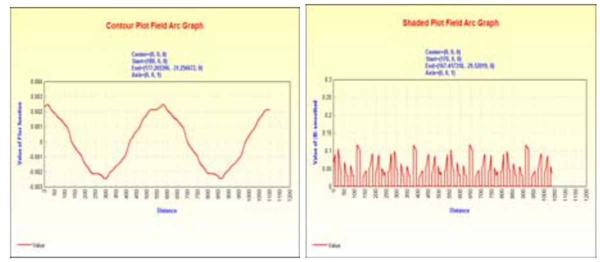

(a)

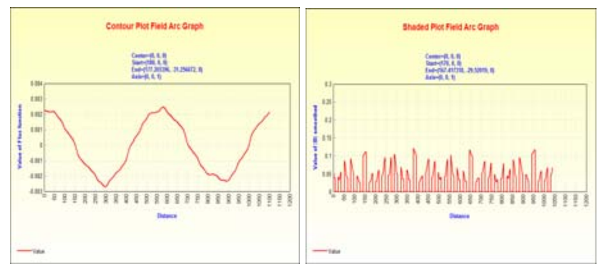

(b)

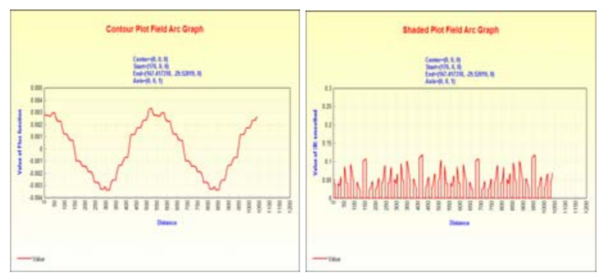

(c)

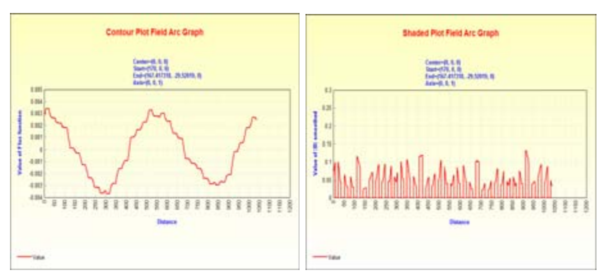

(d)

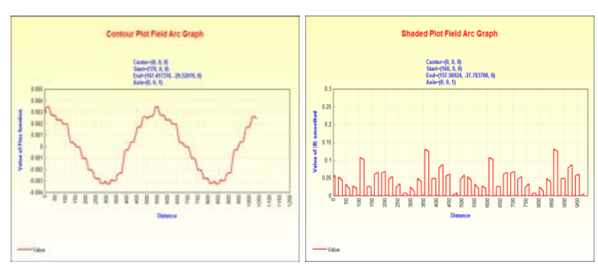

(e)

Figure-4. Field and flux distribution under no load (a) Healthy (b) 2 broken bar (c) 4 broken bar (d) 6 broken bar (e) 8 broken bar.

ARPN Journal of Engineering and Applied Sciences

www.arpnjournals.com

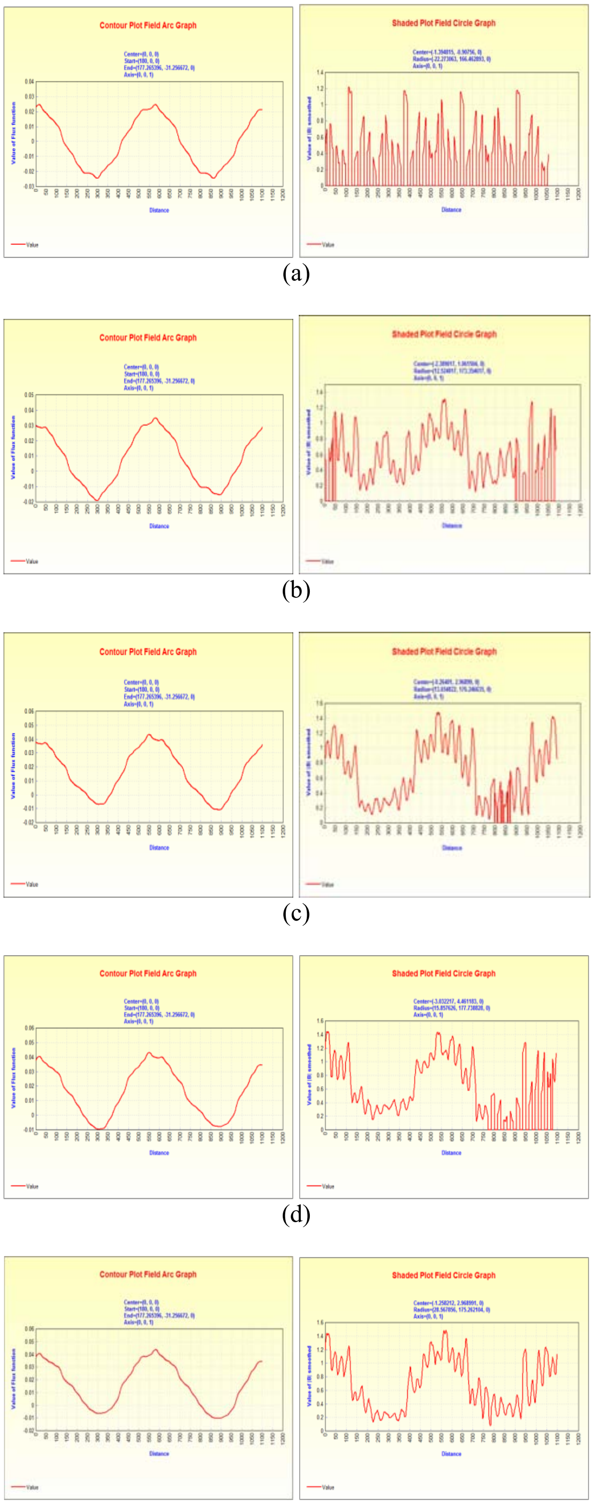

(a) (b) (c) (d) (e)

Figure-5. Field and flux distribution under half load (a) Healthy (b) 2 broken bar (c) 4 broken bar (d) 6 broken bar (e) 8broken bar.

It is observed that the amplitude of the flux function under no load for healthy condition is 0.023 Wb and under faulty condition with two-broken bars is 0.0025 Wb, with four-broken bars is 0.0032 Wb, with six-broken bars is 0.0034 Wb and with eight-broken bars is 0.0035 Wb.

Table-3. Flux function.

Condition		**Flux function** (Wb)	**Percentage change** (%)
No load	Healthy	0.0023	-
	2 broken bar	0.0025	8.69
	4 broken bar	0.0032	39.13
	6 broken bar	0.0034	47.82
	8 broken bar	0.0035	52.17
Half load	Healthy	0.0115	-
	2 broken bar	0.0131	13.91
	4 broken bar	0.0141	22.60
	6 broken bar	0.0157	36.52
	8 broken bar	0.0191	66.08
Full load	Healthy	0.0229	-
	2 broken bar	0.0348	51.96
	4 broken bar	0.0428	86.89
	6 broken bar	0.0432	88.64
	8 broken bar	0.0435	89.95

Similarly, the amplitude for flux density under no load for healthy condition is 0.1229 Wb/m^2 and under faulty condition with two-broken bars is 0.1250 Wb/m^2, with four-broken bars is 0.1298 Wb/m^2, with six-broken bars is 0.1363 Wb/m^2 and with eight-broken bars is 0.1401 Wb/m^2. Similarly it is continued for half and full load.

Table-4. Flux density

Condition		**Flux density** (Wb/m²)	**Percentage change** (%)
No load	Healthy	0.1229	-
	2 broken bar	0.1250	1.70
	4 broken bar	0.1298	5.61
	6 broken bar	0.1363	10.90
	8 broken bar	0.1401	13.99
Half load	Healthy	0.8532	-
	2 broken bar	0.9061	6.20
	4 broken bar	0.9548	11.90
	6 broken bar	1.0043	12.89
	8 broken bar	1.0425	22.18
Full load	Healthy	1.2278	-
	2 broken bar	1.3745	11.94
	4 broken bar	1.4830	21.03
	6 broken bar	1.4861	20.78
	8 broken bar	1.5032	22.43

VOL. 7, NO. 9, SEPTEMBER 2012 ISSN 1819-6608
ARPN Journal of Engineering and Applied Sciences

From the above analysis, it is clear that the amplitude of flux function and flux density increases as the number of broken bars increases. There is a drastic increase in flux function and flux density when the load increases from no load to full load. Also when the number of broken bars increased from two broken bars to eight broken bars, the flux function and flux density increases and respective percentage change is obtained.

TRANSIENT ANALYSIS

In this section, the simulation results for the Transient Analysis of Three Phase Induction Motor for healthy motor, faulty motor with 2, 4, 6 and 8 broken bars under no load, and full load are presented.

Transient model of induction motor

The electrical model representation of three phase squirrel cage star connected induction motor is shown in Figure-6. The power source is considered as a voltage source connected with the series resistances and inductances of the stator windings in each phase.

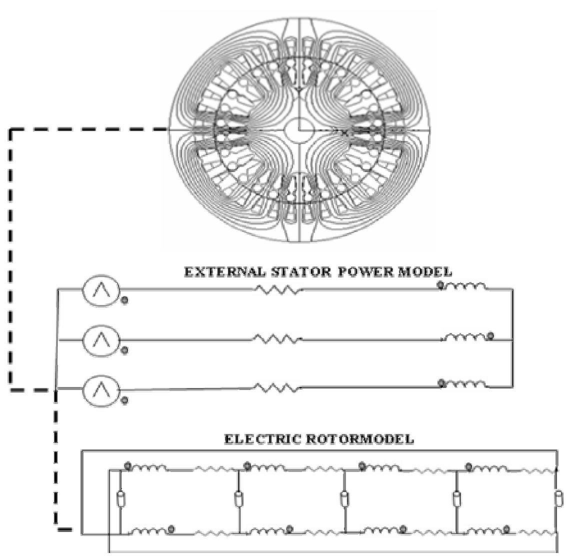

Figure-6. Transient model of induction motor.

The rotor circuit model is made of short-circuited bar conductors. The circuit model of the three phase induction motor is shown in Figure-7.

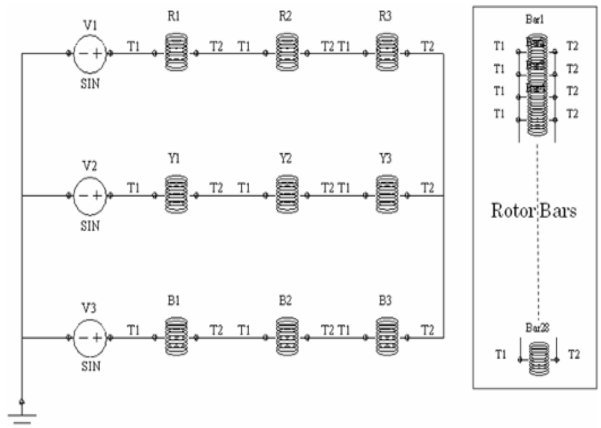

Figure-7. Electric circuit model of induction motor.

The voltage relations for all the phases are defined as:

$$V_1 = V_m \sin wt \quad (2)$$

$$V_2 = V_m \sin (wt-2\pi/3) \quad (3)$$

$$V_3 = V_m \sin (wt+2\pi/3) \quad (4)$$

Instantaneous magnetic energy plot

When electric current flows in an inductor, energy is stored in the magnetic field. The instantaneous magnetic energy plot for healthy and faulty motor under no load is shown in Figure-8, under full load is shown in Figure-9.

The time step is taken as 10ms. The instantaneous energy at the starting instant is found to be high and gradually decreases to attain a steady value when the time is increased to 4000 ms.

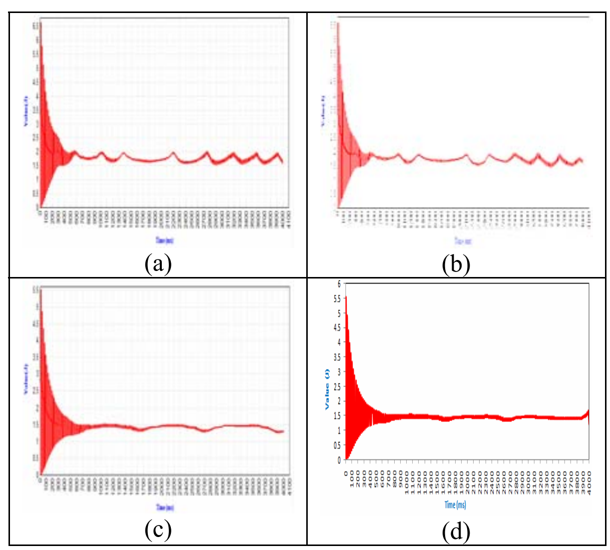

ARPN Journal of Engineering and Applied Sciences

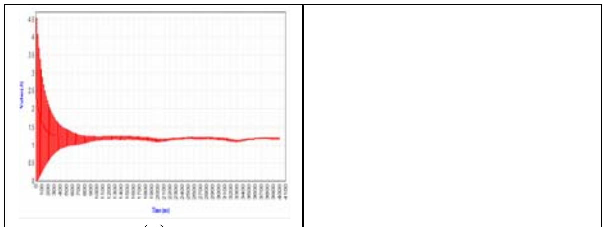

(e)

Figure-8. Instantaneous magnetic energy under no load (a) Healthy (b) 2 broken bar (c) 4 broken bar (d) 6 broken bar (e) 8broken bar.

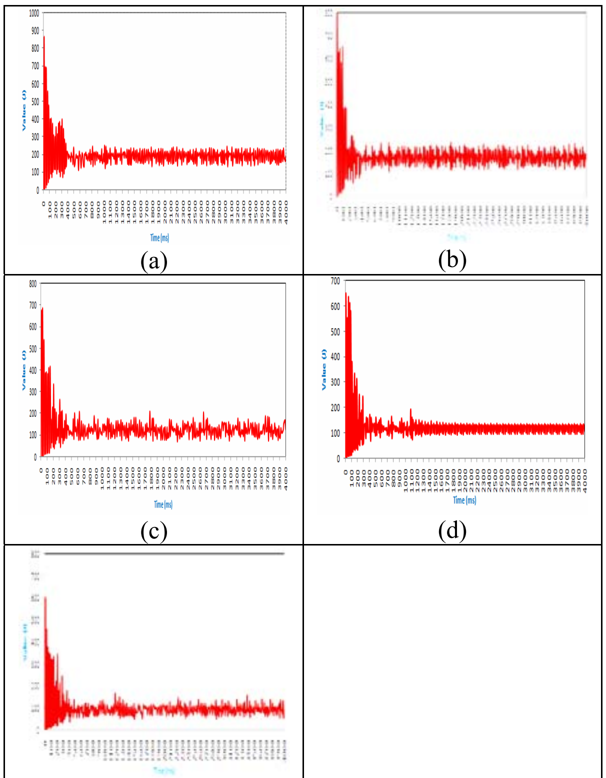

(a) (b) (c) (d) (e)

Figure-9. Instantaneous magnetic energy under full load (a) Healthy (b) 2 broken bar (c) 4 broken bar (d) 6 broken bar (e) 8broken bar.

The instantaneous magnetic energy values under various load are tabulated in Table-5. Under no load, the instantaneous magnetic energy for healthy is 1.58446 Joules, for 2 broken bars is 1.57958 Joules, for 4 broken bars is 1.28950 Joules, for 6 broken bars is 1.21112 Joules and for the 8 broken bars is 1.16965 Joules. Under full load, the instantaneous magnetic energy for healthy is 194.2153 Joules, for 2 broken bars is 157.6726 Joules, for 4 broken bars is 125.8326 Joules, for 6 broken bars is 107.2033 Joules and for the 8 broken bars is 91.4319 Joules. The graphical representation for Instantaneous magnetic energy is shown in Figure-10.

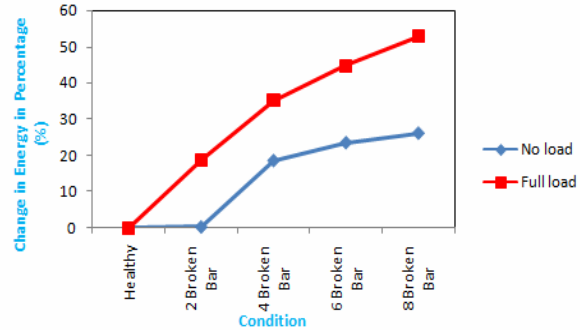

Figure-10. Instantaneous magnetic energy- graphical representation.

Table-5. Instantaneous magnetic energy.

Condition		**Instantaneous magnetic energy** (Joules)	**Percentage change** (%)
No load	Healthy	1.58446	-
	2 broken bar	1.57958	0.307
	4 broken bar	1.28950	18.61
	6 broken bar	1.21112	23.56
	8 broken bar	1.16965	26.17
Full load	Healthy	194.2153	-
	2 broken bar	157.6726	18.81
	4 broken bar	125.8326	35.20
	6 broken bar	107.2033	44.80
	8 broken bar	91.4319	52.92

Hence the above analysis shows that there is an increase in the percentage change when the broken bars increase. Hence this observation shows that the instantaneous magnetic energy decreases as the broken bars increases.

Stator phase current plot

The stator phase current plot for healthy and faulty motor under no load is shown in Figure-11 and for full load is shown in Figure-12. The time step is taken as 10ms.

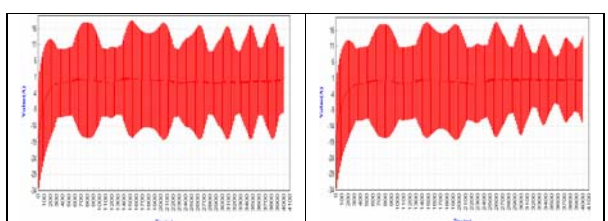

(a) (b)

VOL. 7, NO. 9, SEPTEMBER 2012 ISSN 1819-6608
ARPN Journal of Engineering and Applied Sciences

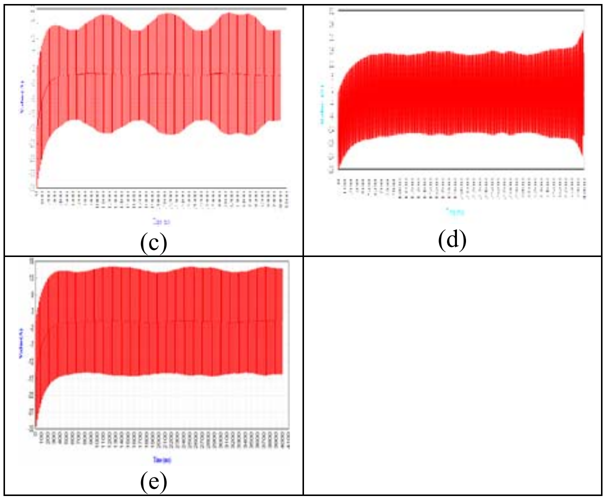

Figure-11. Stator phase current under no load (a) Healthy (b) 2 broken bar (c) 4 broken bar (d) 6 broken bar (e) 8broken bar.

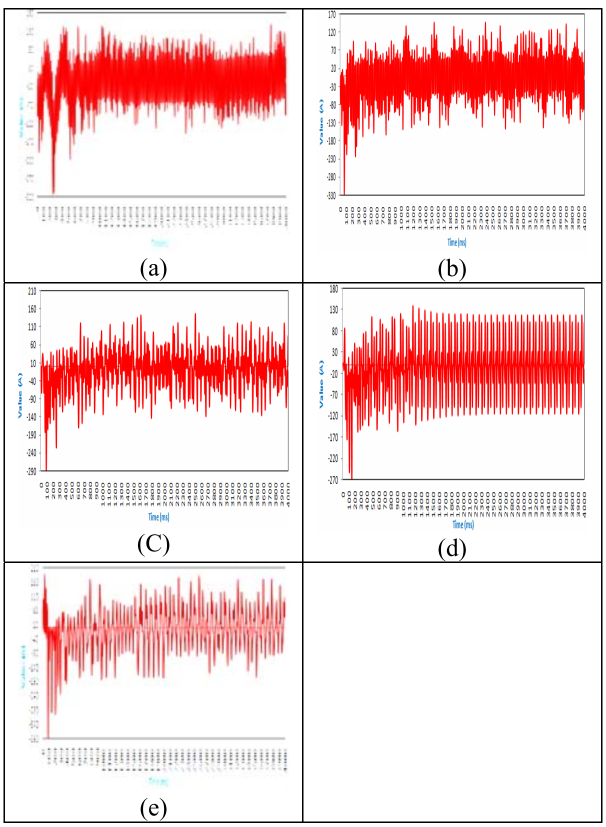

Figure-2. Stator phase current under full load (a) Healthy (b) 2 broken bar (c) 4 broken bar (d) 6 broken ba (e) 8 broken bar.

The stator phase current values under various loads are tabulated in Table-6. Under no load, the current obtained for healthy is 10.40 A, for 2 broken bars is 14.13 A, for 4 broken bars is 14.87 A, for 6 broken bars is 15.07 A and for the 8 broken bars is 15.79 A. Under full load, the current obtained for healthy is 57.23 A, for 2 broken bars is 69.97 A, for 4 broken bars is 84.30 A, for 6 broken bars is 98.35 A and for the 8 broken bars is 106.90 A.

Table-6. Stator phase current.

Condition		**Stator phase current** (A)	**Percentage change** (%)
No load	Healthy	10.40	-
	2 broken bar	14.13	35.86
	4 broken bar	14.87	42.96
	6 broken bar	15.07	44.89
	8 broken bar	15.79	51.79
Full load	Healthy	57.23	-
	2 broken bar	69.97	22.25
	4 broken bar	84.30	47.29
	6 broken bar	98.34	71.83
	8 broken bar	106.9	86.78

Hence the above analysis show that the stator phase current increases as the broken bars increases.

Flux linkage plot

The flux linkage plot for healthy and faulty motor under no load is shown in Figure-13 and for full load is shown in Figure-14. The time step is taken as 10ms. The flux linkage values under various loads are tabulated in Table-7.

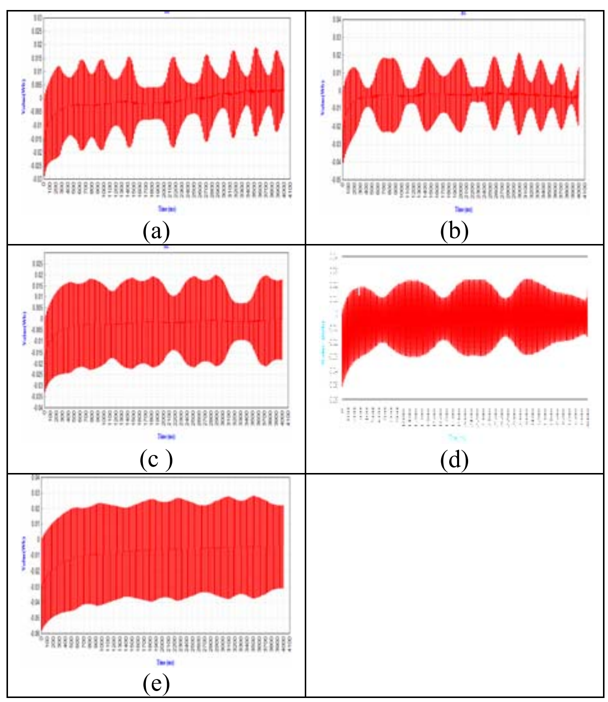

Figure-13. Flux linkage under no load (a) Healthy (b) 2 broken bar (c) 4 broken bar (d) 6 broken bar (e) 8 broken bar.

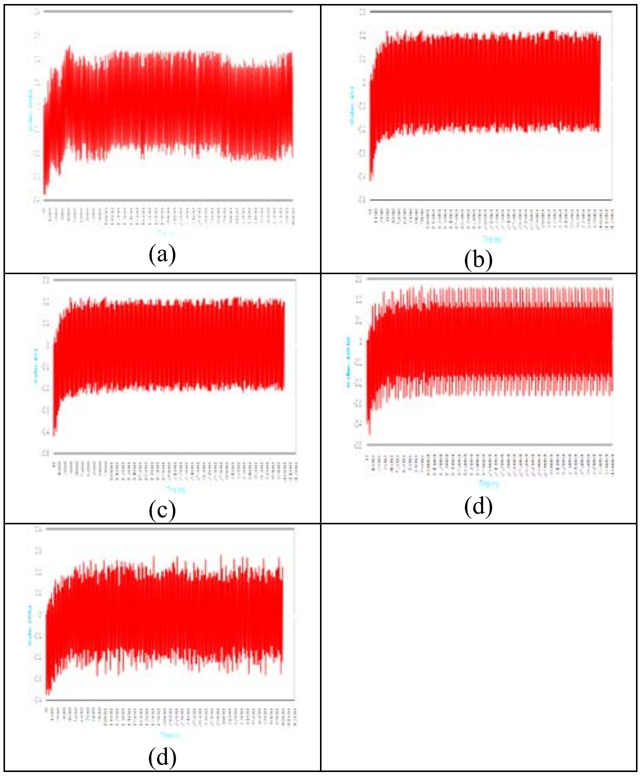

Figure-14. Flux linkage under full load (a) Healthy (b) 2 broken bar (c) 4 broken bar (d) 6 broken bar (e) 8 broken bar

It can be observed that under no load, the flux linkage obtained for healthy is 0.01104 Wb, for 2 broken bars is 0.01327 Wb, for 4 broken bars is 0.01791 Wb, for 6 broken bars is 0.01822 and for 8 broken bars is 0.02205 Wb. Under full load, the flux linkage obtained for healthy is 0.16668 Wb, for 2 broken bars is 0.19386 Wb, for 4 broken bars is 0.22034 Wb, for 6 broken bars is 0.25851 Wb and for 8 broken bars is 0.31012 Wb.

Table-7. Flux linkage.

Condition		**Flux Linkage** (Wb)	**Percentage change** (%)
No load	Healthy	0.01104	-
	2 broken bar	0.01327	20.19
	4 broken bar	0.01791	62.22
	6 broken bar	0.01822	65.04
	8 broken bar	0.02205	99.72
Full load	Healthy	0.16668	-
	2 broken bar	0.19386	16.30
	4 broken bar	0.22034	32.19
	6 broken bar	0.25851	55.09
	8 broken bar	0.31012	86.05

Hence it is observed that the value of flux linkage increases when the number of broken bars increases.

Magnetic torque plot

The Magnetic Torque has been increased when the number of broken bars was increased. The value for Magnetic Torque is tabulated in Table-8. It can be observed that under no load the magnetic torque obtained for healthy motor is 1.4562 Nm, for 2 broken bars is 2.0683 Nm, for 4 broken bars is 2.5302 Nm, for 6 broken bars is 2.7809 Nm and for 8 broken bars is 2.8211 Nm. Under full load the magnetic torque obtained for is 123.684 Nm, for 2 broken bars is 161.468 Nm, for 4 broken bars is 187.245 Nm, for 6 broken bars is 207.047 Nm and for 8 broken bars is 225.006 Nm.

Table-8. Magnetic torque.

Condition		**Magnetic torque** (Nm)	**Percentage change** (%)
No load	Healthy	1.4562	-
	2 broken bar	2.0683	42.03
	4 broken bar	2.5302	73.75
	6 broken bar	2.7809	90.96
	8 broken bar	2.8211	93.73
Full load	Healthy	123.684	-
	2 broken bar	161.468	30.54
	4 broken bar	187.245	51.38
	6 broken bar	207.047	67.39
	8 broken bar	225.006	81.92

The graphical representation for Magnetic Torque is shown in Figure-15.

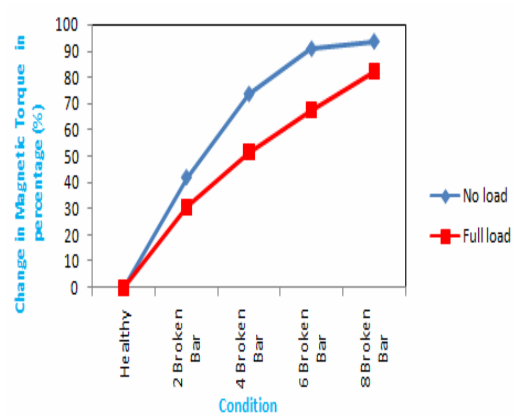

Figure-15. Magnetic torque-graphical representation.

Hence the above analysis shows that there is an increase in the percentage change when the broken bars increase.

CONCLUSIONS

A three phase squirrel cage induction motor is modeled on the basis of finite element method. The simulation result was obtained for broken bar faults. Comparisons are made with the healthy motor condition and the result was tabulated. It was found that the faults due to the broken bars saturate the magnetic field distribution on the rotor tooth adjacent to the bars that were broken. In the static analysis, the stored magnetic energy decreased when the number of broken bars increased. The Flux Function and Flux Density was increased when the number of broken bars was increased. In the transient analysis, it was found that the flow of current in the stator phases and the flux linkage produced in the motor was increased, whereas, the stored magnetic energy was decreased when the number of broken bars was increased. Also the magnetic torque was increased when the number of broken bars was increased. The simulated results are verified theoretically for the values like flux function and flux density.

REFERENCES

[1] Balamurugan S., Arumugam R., Paramasivam S. and Malaiappan M. 2004. Transient Analysis of induction Motor Using Finite Element Analysis. IEEE Industrial Electronics Society, 30th annual conference. pp. 1526-1529.

[2] John.F. Bangura, Richard J. Povinelli, Nabeel A. O. Demerdash and Ronald H. Brown. 2003. Diagnostics of Eccentricities and Bar/End-Ring Connector Breakages in Polyphase Induction Motors through a combination of Time-Series Data Mining and Time Stepping Coupled FE - State Space Technique. IEEE Trans. on Industrial Applications. 39(4): 1005-1013.

[3] Bentounsi A. and Nicolas A. 1998. On Line Diagnosis of Defaults on Squirrel Cage Motor Using FEM. IEEE Trans. Magn. 34(5): 3511-3574.

[4] Bianchi N., Bolognani S. and Comelato G. 1999. Finite Element Analysis of Three Phase Induction Motors: Comparison of Two Different Approaches. IEEE Trans. on Energy Conversion. 14(4): 1523-1528.

[5] Elkasabgy N. M. and Eastham A. R. 1992. Detection of Broken Bars in the Cage Rotor on an Induction Machine. IEEE Trans. Ind. Appl. 28(1): 165-171.

[6] Genadi Y. Sizov and Ahmed Sayed-Ahmed nabeel. 2009. Analysis and Diagnostics of Adjacent and Nonadjacent Broken-Rotor-Bar Faults in Squirrel-Cage Induction Machines. IEEE Trans. on Industrial Electronics. 56(11): 4627-4641.

[7] Jee-Hoon Jung and Bong-Hwan Kwon. 2006. Corrosion Model of a Rotor Bar under Fault Progress in Induction Motors. IEEE Trans. on Industrial Electronics. 53(6): 1829-1841.

[8] Li Weili, XieYing, Shen Jiafeng and Luo Yingli. 2007. Finite Element Analysis of Field Distribution and Characteristic Performance of Squirrel-Cage Induction Motor with Broken Bars. IEEE Trans. on Magnetics. 43(4): 1537-1540.

[9] Manuel Pineda-Sanchez, Riera-Guasp. M, Jose A. Antonino-Daviu, Roger-Folch J., Perez-Cruz J. and Puche-Panadero R. 2010. Diagnosis of Induction motor faults in the Fractional Fouries Domain. IEEE Trans. on Instrumentation and Measurement. 59(8): 2065-2075.

[10] Mirafzal B. and Demerdash N. A. O. 2004. Induction Machine Broken-Bar Fault Diagnosis Using the Rotor Magnetic Field Space-Vector Orientation. IEEE Trans. Ind. Appl. 40(2): 534-542.

[11] Mohammed O.A., Abed N.Y. and Ganu S. 2007. Modeling and Characterization of induction motor internal faults using Finite Element and Discrete Wavelet Transforms. IEEE 2007. pp. 250-253.

[12] Preston T. W., Reece A. B. J. and Sangha P. S. 1988. Induction Motor Analysis by Time-Stepping Techniques. IEEE Trans. on Magnetics. 24(1): 471-474.

[13] Subhasis Nandi, Shehab Ahmed and Hamid A. Toliyat. 2001. Detection of Rotor Slot and other Eccentricity Related Harmonics in a Three Phase Induction Motor with different rotor cages. IEEE Trans. on Energy Conversion. 16(3): 253-260.

[14] Vaseghi B., Takorabet N. and Meibody-Tabar F. 2008. Modeling of 1M with Stator Winding Inter-turn Fault Validated by FEM. Proceedings of the 2008 International Conference on Electrical Machines.

[15] William T. Thomson and Mark Fenger. 2001. Current Signature Analysis to detect Induction Motor Faults. IEEE Industry Application Magazine. pp. 26-34.

[16] Zou Zou S.E. 2010. Detection of Inter-Turn Short-Circuit and broken Rotor Bars in Induction Motors Using the Partial Relative Indexes: Application on the MCSA. Int. Conf.

[17] Sawhney A. K. A Course in Electrical Machine Design. Dhanpat Rai and Sons.